Int J Adv Manuf Technol (2017) 92:4081–4093
DOI 10.1007/s00170-017-0427-6

ORIGINAL ARTICLE

Mode decoupled and sensorless cutting force monitoring based on multi-encoder

Yuki Yamada[1] · **Shuntaro Yamato**[1] · **Yasuhiro Kakinuma**[1]

Received: 30 January 2017 / Accepted: 12 April 2017 / Published online: 10 May 2017

Abstract Cutting force monitoring is an important technology for tool condition monitoring. However, a high precision and wideband cutting force estimation, including cross-feed components, with a sensorless approach of the ball-screw-driven stage, is still challenging because of its multiple structural modes and non-linear friction. This study proposes a process monitoring technique that independently estimates the cutting force components in rigid body and in vibration mode coordinate systems, based on multi-encoder signals. In the rigid body mode, the cutting force components were estimated by extracting the static rigid-body motion. In the vibration mode, the cutting force was estimated by using the relative displacement, velocity, and acceleration between the motor and the table. The estimation accuracy of the cutting force in feed and cross-feed directions was evaluated through several end milling tests. In the rigid body mode, a temporal variation of the feed force components was observed. However, high-frequency variations irrelevant to the cutting force were included because of variations in motor current, which had position/rotation-dependent characteristics. On the other hand, in the vibration mode, it was possible to estimate both feed and cross-feed components with less than maximum static friction force, including high harmonics.

Keywords Process monitoring · Ball-screw-driven stage · Sensorless · Mode decoupling · Multi-encoder-based disturbance observer

✉ Yuki Yamada
yamada@ams.sd.keio.ac.jp

[1] Department of System Design Engineering, Keio University, 3-14-1 Hiyoshi, Kohoku-ku, Yokohama 223-8522, Japan

Nomenclature

a_t	Acceleration of table
$a_m(=R\alpha_m)$	Equivalent value of α_m in translational motion
C_t	Viscous friction coefficient of transl. element
C_k	Damping coefficient of structure
$C_r(=D_r/R^2)$	Equivalent value of D_r in translational motion
D_r	Viscous friction coefficient of rotational element
F_{cut}	Cutting force
F_{fric}	Friction force
I_a	Motor current
I_a^{comp}	Compensation current for disturbance force
J_r	Total inertia of motor, coupling, and ball-screw
K_r	Total rigidity of feed screw system
K_t	Torque coefficient
ℓ	Pitch length
M_t	Movable mass
$M_r(=J_r/R^2)$	Equivalent value of J_r in transl. motion
R	Transform coefficient for rotational to translational motion ($=\ell/2\pi$)
T_{fric}	Friction torque
T_a , T_b	Identified dead time
T_{comp}	Dead time for phase lag compensation
x_t	Displacement of table
$x_m(=R\theta_m)$	Equivalent value of θ_m in translational motion
v_t	Velocity of table
$v_m(=R\omega_m)$	Equivalent value of ω_m in translational motion
$\alpha(=M_t/M_r)$	Inertia ratio
α_m	Angular acceleration
α_c , β_c	Constant for proportional damping
θ_m	Angle of motor
ω_m	Angular velocity of motor
ω_{cc}	Bandwidth of current loop
^(hat)	Estimated value

Matrix and vector

$\boldsymbol{x}, \boldsymbol{v}, \boldsymbol{a}$	Displacement, velocity, and acceleration vector
$\boldsymbol{M}, \boldsymbol{C}, \boldsymbol{K}$	Mass, damping, stiffness matrix
$\boldsymbol{F}$	Force vector
ϕ	Modal matrix

Subscript

modal	Value in modal coordinate system
n	Nominal value
rigid	Value in rigid body mode
vib	Value in vibration mode

Superscript

cmd	Command value
ref	Reference value
res	Response value

1 Introduction

In the manufacturing field, an intelligent technique for enhancing productivity has been developed based on the sensor-based condition monitoring. Tool condition monitoring has drawn attention, because it is closely related to the dynamics of the cutting process [1]. In particular, the cutting force is one of the most valuable cutting process-related indicators [2]; therefore, a condition monitoring technique focused on the cutting force has been developed. Measurements of a cutting force could be broadly classified into two categories, namely, direct and indirect measurements. The direct cutting force measurement, using a piezoelectric quartz dynamometer, is well established as the de-facto standard. However, the use of dynamometers significantly increases initial costs, has a limitation regarding installation size, and decreases the loop stiffness from tool to workpiece. Thus, in most situations, dynamometers are restricted to research applications.

Indirect cutting force measuring techniques could be categorized into two types, sensor-based and sensorless. In the sensor-based techniques, displacement sensors are often attached to the spindle, and the cutting force is estimated by the variation of position that it causes. Because the sensors are attached to the spindle, the measurements are not influenced by the mass variation of the workpiece, in contrast with measurements using the dynamometer. Albrecht et al. [3] compensated the dynamics between tool and sensors using the Kalman filter and enhanced the estimation bandwidth to approximately 1 kHz. Sarhan and Matsubara et al. [4] considered the change in thermal deformation and stiffness resulting from the high-speed rotation of the spindle. Albertelli et al. [5] estimated the cutting force as well as tool tip vibration in relation to the surface-quality of the machined workpiece. Although the cutting force could be estimated accurately by using additional sensors, a decrease in reliability and increase in the maintenance cost are inevitable with the increasing number of sensors employed. The reduction in maintainability is noteworthy when sensors are embedded inside the spindle.

Sensorless cutting force monitoring using inner information of the machine tools has drawn attention because of its sustainability. Altintas et al. [6] established a cutting force monitoring methodology for a DC servo motor, and Lee et al. [7] extended it to an AC servo drive. Based on this methodology, current signals of the feed drive could be used for sensing the cutting force in the feed direction within the bandwidth of the current control loop. For example, bandwidth of the current sensor in [6] and [7] is approximately 20 and 62 Hz, respectively. If an observer is established using position/angle in addition to current signal, the estimation bandwidth and accuracy could be enhanced. Shinno et al. [8] successfully monitored the cutting force without the influence of variation in temperature, unlike the case with the dynamometer. Takei and Kakinuma et al. [9] showed that cutting force monitoring surpassing the current control bandwidth was feasible in a linear motor-driven stage. In the ball-screw-driven stage, however, high precision and wideband cutting force estimation is more difficult because of the existing multiple structural modes and non-linear friction. The friction force/torque changed significantly according to the feed rate, table position, workpiece mass, and the use of chip cover [10], while the position-dependent fluctuation of friction was highly repeatable [11]. Particularly in milling, cutting force monitoring, including not only the fundamental frequency component but also its harmonics, is required, because they could result in the development of chatter. In many studies, monitoring performance of cutting forces was discussed at slotting. A few studies dealt with monitoring performance at a low radial immersion, where cutting processes became more intermittent.

A sensorless estimation technique for the cross-feed (i.e., stationary feed) direction components of the cutting force is also important, because they directly affect the quality of the machined surface. However, the following error factors distort the current signal and make it difficult to estimate the cutting force in cross-feed direction [12]: the stick-slip friction, lower encoder resolution, and arbitrary property of the stationary feed motor current. Jeong and Cho [12] asserted that the stationary feed motor current was influenced by the magnitude and frequency of the cutting force. In addition, they mentioned that the cutting force could be estimated if the stick-slip friction is assumed as a constant influence. Ibaraki et al. [13] proposed an estimation scheme by geometrically combining the force vectors given by the servo motor and spindle motor currents. The armature current in a spindle motor, which is less affected by the non-linearity of friction, was used for estimating only the tangential component of cutting force. The validity of the proposed method was evaluated through end milling tests with vertical machining centers, with both sliding and rolling guideways. However, the cutting force estimation

was quasi-static due to the rigid body-based formulation. Sato et al. [14] extracted the cutting force components included in motor current by an inverse transformation from frequency to time domain. The cutting force components in cross-feed direction were successively estimated when the cutting force became larger than the static friction force.

In our previous study [15], we developed a sensorless cutting force estimation method based on the multi-encoder-based disturbance observer (MEDOB) [16]. In the method, the feed force components were estimated by using the servo signals of a full-closed controlled ball-screw-driven stage: the motor current reference, the rotation angle of the motor, and the displacement of the stage. The effect of the position-dependent friction on force estimation was reduced by identifying the friction force/torque under the same position trajectory and velocity as cutting. By integrating a linear encoder signal into the observer, which was close to the cutting point, more wideband cutting force estimation was possible than current reference monitoring.

In this study, a process monitoring technique is proposed by independently estimating the cutting force components in the rigid body mode and in the vibration mode coordinate systems, based on multi-encoder signals. The cutting force was estimated from the servo signals of a full-closed controlled ball-screw-driven stage. By conducting an experimental modal analysis, the two mutually orthogonal modes were introduced from the dual-inertia model of the ball-screw-driven stage. By extracting the static rigid body motion, it is feasible to estimate the cutting force component independently from the non-linear stiffness variation that corresponds to the machine's configuration in the rigid body mode. In addition, cutting force monitoring in the rigid body mode is theoretically identical to MEDOB-based cutting force monitoring. In the vibration mode, the dynamic variation of cutting force could be monitored in the dynamic coordinate system based on relative displacement, velocity, and acceleration. The proportion of motor current reference in the estimated force can be lowered when the inertia ratio is less than 1, which contributes to highly accurate cutting force estimation in cross-feed direction. Furthermore, the monitoring accuracy of a dynamically abnormal state, such as chatter or tool fracture, could be enhanced. This study focused on estimating variable components of the cutting force rather than DC component. As for the friction force/torque, DC component was more dominant than variable components, while they had position-dependent and repeatable characteristics. In order to keep conciseness of this paper, the influence of the friction terms on the cutting force estimation was eliminated by conducting idling test instead of developing a dynamic model. The validity of the proposed monitoring method was experimentally evaluated through several end milling tests where feed rate and direction were constant. Phase lag in the control system and friction force/torque were identified and compensated in a similar manner to our past study [15]. Estimation performance under reciprocal motions with changing direction of friction was not evaluated in this study, while estimation accuracy of the static component could be influenced by the motions. Because the cutting force was monitored in the equivalent single-degree-of-freedom (SDOF) system, the proposed method is applicable to existing process monitoring techniques established for the SDOF system. In addition, the basic idea of the proposed method is also applicable to sensor-based cutting force monitoring.

2 Methodology

2.1 Experimental setup

Figure 1 shows the prototype of a three-axis ball-screw-driven machine tool. AC servomotors are used as actuators, and shaft and screws are directly connected by couplings. The ball-screws are doubly anchored with support bearings. The pitch length of the screw is 5 mm, and the stage is supported by rolling guideways. Although the proposed estimation technique can be implemented in the control system of all axes, in this study, the estimation performance was verified in the *X*-axis direction, at the workpiece side, which can be compared with the result of a dynamometer. The system configuration of the cutting force estimation is shown in Fig. 2. Feedback signals for the position/velocity controller are provided by a linear encoder attached to the table (LIF481R, from HEIDENHAIN) and a rotary encoder (resolution: 23 bit) built into the motor. The rotary encoder had a 512 ($=2^9$) count/rev signal period and the signal was interpolated 16,384 ($=2^{14}$)

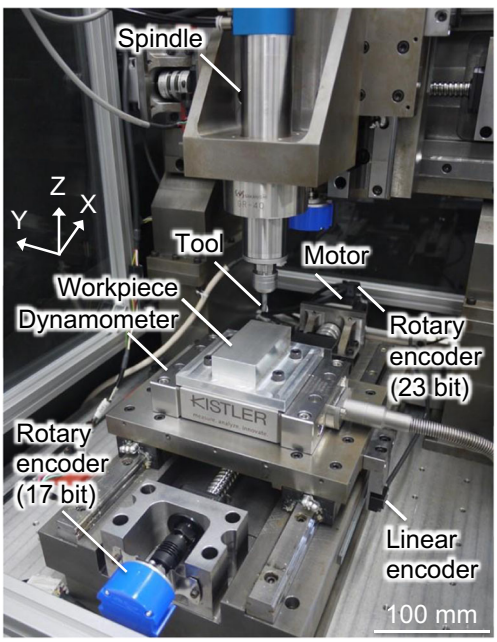

Fig. 1 Experimental setup

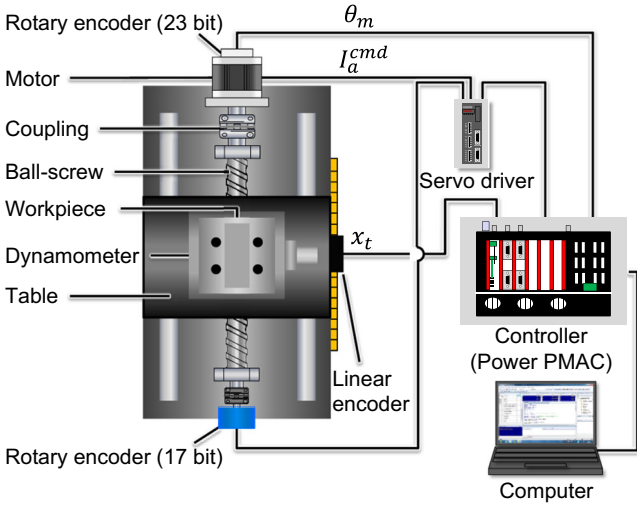

Fig. 2 System configuration for cutting force estimation

times. The linear encoder had a 4-μm signal period and provided a resolution of 244 pm by interpolating 16,384 times. High-resolution encoders were used in order to reduce measurement errors of velocity and acceleration, which were used in the cutting force estimation. The current control loop was implemented in servo driver. At the counter-motor side, another rotary encoder (resolution: 17 bit) was mounted, which was not used for cutting force estimation but for generating the electrical angle of the servomotors.

Current reference signals were generated from a motion controller (Power PMAC, from Delta Tau). Both the sampling frequency of data acquisition and the updating frequency of the current reference were set at 10 kHz. For comparison, a dynamometer (type 9129A, from Kistler) was mounted on the table to measure the cutting forces.

2.2 Mode decoupled cutting force estimation method based on dual-inertia model

A cutting force estimating equation is introduced based on the dual-inertia model of the ball-screw-driven stage shown in Fig. 3. This model is simpler and more intuitive than high-order model, which is beneficial in terms of actual use. In addition, the number of degree of freedom coincides with that of sensors in the ball-screw-

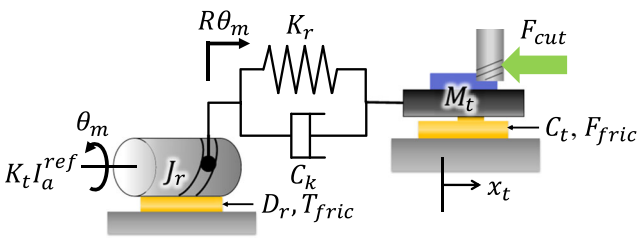

Fig. 3 Dual-inertia model of ball-screw-driven stage

driven stage with full-closed controlled. The dynamic equations are as follows:

$$\begin{bmatrix} J_r & 0 \\ 0 & M_t \end{bmatrix} \begin{Bmatrix} \alpha_m \\ a_t \end{Bmatrix} + \begin{bmatrix} D_r + C_k R^2 & -C_k R \\ -C_k R & C_t + C_k \end{bmatrix} \begin{Bmatrix} \omega_m \\ v_t \end{Bmatrix} + \begin{bmatrix} K_r R^2 & -K_r R \\ -K_r R & K_r \end{bmatrix} \begin{Bmatrix} \theta_m \\ x_t \end{Bmatrix} = \begin{Bmatrix} K_t I_a^{\text{ref}} - T_{\text{fric}} \\ -F_{\text{fric}} - F_{\text{cut}} \end{Bmatrix} \quad (1)$$

Here, current reference, I_a^{ref}, and current response, I_a^{res}, were regarded as equivalent for simplification. By transforming the dynamic equation in rotational motion to translational motion, Eq. (1) is rewritten as follows:

$$[\boldsymbol{M}]\{\boldsymbol{a}\} + [\boldsymbol{C}]\{\boldsymbol{v}\} + [\boldsymbol{K}]\{\boldsymbol{x}\} = \{\boldsymbol{F}\} \quad (2)$$

where

$$[\boldsymbol{M}] = \begin{bmatrix} M_r & 0 \\ 0 & M_t \end{bmatrix}, [\boldsymbol{C}] = \begin{bmatrix} C_r + C_k & -C_k \\ -C_k & C_t + C_k \end{bmatrix},$$

$$[\boldsymbol{K}] = \begin{bmatrix} K_r & -K_r \\ -K_r & K_r \end{bmatrix}, \{\boldsymbol{a}\} = \begin{Bmatrix} a_m \\ a_t \end{Bmatrix}, \{\boldsymbol{v}\} = \begin{Bmatrix} v_m \\ v_t \end{Bmatrix},$$

$$\{\boldsymbol{x}\} = \begin{Bmatrix} x_m \\ x_t \end{Bmatrix}, [\boldsymbol{F}] = \begin{Bmatrix} K_t I_a^{\text{ref}} \big/ R - T_{\text{fric}} \big/ R \\ -F_{\text{fric}} - F_{\text{cut}} \end{Bmatrix}$$

In this study, proportional damping (i.e., $[\boldsymbol{C}] = \alpha_c[\boldsymbol{M}] + \beta_c[\boldsymbol{K}]$, $\alpha_c = C_r/M_r = C_t/M_t$, $\beta_c = C_k/K_r$) was considered. To decouple the dual-inertia model, the following modal transformation was conducted:

$$\{\boldsymbol{x}\} = [\phi]\{\boldsymbol{x}_{\text{modal}}\} \quad (3)$$

where

$$[\phi] = \begin{bmatrix} 1 & 1 \\ 1 & -1/\alpha \end{bmatrix}, \{\mathbf{x}_{\text{modal}}\} = \begin{Bmatrix} x_{\text{rigid}} \\ x_{\text{vib}} \end{Bmatrix} = \frac{1}{\alpha + 1} \begin{Bmatrix} x_m + \alpha x_t \\ \alpha(x_m - x_t) \end{Bmatrix}$$

The modal transformation is applicable to $\{\boldsymbol{v}\}$ and $\{\boldsymbol{a}\}$. By multiplying $[\phi]^T$ on the left side of Eq. (2), a decoupled dynamic equation is introduced as follows:

$$[\boldsymbol{M}_{\text{modal}}]\{\boldsymbol{a}_{\text{modal}}\} + [\boldsymbol{C}_{\text{modal}}]\{\boldsymbol{v}_{\text{modal}}\} + [\boldsymbol{K}_{\text{modal}}]\{\boldsymbol{x}_{\text{modal}}\} = [\phi]^T\{\mathbf{F}\} \quad (4)$$

where

$$[\boldsymbol{M}_{\text{modal}}] = [\phi]^T[\boldsymbol{M}][\phi] = \begin{bmatrix} M_r + M_t & 0 \\ 0 & \left(1 + 1/\alpha\right) M_r \end{bmatrix} = \begin{bmatrix} M_{\text{rigid}} & 0 \\ 0 & M_{\text{vib}} \end{bmatrix}$$

$$[\boldsymbol{C}_{\text{modal}}] = [\phi]^T[\boldsymbol{C}][\phi] = \alpha_c[\boldsymbol{M}_{\text{modal}}] + \beta_c[\boldsymbol{K}_{\text{modal}}] = \begin{bmatrix} C_{\text{rigid}} & 0 \\ 0 & C_{\text{vib}} \end{bmatrix}$$

$$[\boldsymbol{K}_{\text{modal}}] = [\phi]^T[\boldsymbol{K}][\phi] = \begin{bmatrix} 0 & 0 \\ 0 & \left(1+1/\alpha\right)^2 K_{\text{r}} \end{bmatrix} = \begin{bmatrix} 0 & 0 \\ 0 & K_{\text{vib}} \end{bmatrix}$$

After modal transformation, the non-diagonal elements of $[\boldsymbol{M}_{\text{modal}}]$, $[\boldsymbol{C}_{\text{modal}}]$, and $[\boldsymbol{K}_{\text{modal}}]$ became zero. Because first row, first column of $[\boldsymbol{K}_{\text{modal}}]$ is zero, the first row of Eq. (4) indicates the dynamic equation in the rigid body mode, while the second row does that in the vibration mode. By solving Eq. (4), the estimating equations of cutting force in the rigid body and vibration modes could be denoted as follows:

$$F_{\text{cut(rigid)}} = K_t I_a^{\text{ref}} / R - T_{\text{fric}} / R - F_{\text{fric}} - M_{\text{rigid}} a_{\text{rigid}} - C_{\text{rigid}} v_{\text{rigid}} \tag{5}$$

$$F_{\text{cut(vib)}} = -\alpha\left[K_t I_a^{\text{ref}} / R - T_{\text{fric}} / R + F_{\text{fric}} / \alpha - (M_{\text{vib}} a_{\text{vib}} + C_{\text{vib}} v_{\text{vib}} + K_{\text{vib}} x_{\text{vib}})\right] \tag{6}$$

In practice, a low pass filter is implemented to eliminate higher frequency noise. Because v_{rigid}, a_{rigid}, a_{vib}, v_{vib}, x_{vib} are derived from θ_m and x_t, the cutting force could be estimated based on Eqs. (5) and (6) with adequate identification of friction terms.

As mentioned before, the authors had developed a MEDOB-based cutting force estimation method [15]. In that method, the cutting force could be estimated without using the stiffness value, K_t. On the other hand, the MEDOB-based estimation is essentially the same as the estimation in the rigid body mode. In other words, the stiffness independent estimation was possible in MEDOB, because the rigid body motion of the ball-screw-driven stage was extracted by applying MEDOB. In the Appendix, the equivalence is analytically proved.

As can be seen in Eq. (3), the modal displacement in the vibration mode is calculated from the relative displacement between the stage and the motor. Similarly, the modal velocity and acceleration in the vibration mode are calculated. Thus, the cutting force estimation in vibration mode is based on relative displacement, velocity, and acceleration. Mode decoupling is applicable to analyze the damping property of the relative velocity feedback control system [17].

It is possible to extend the basic idea of the proposed method to a multi-inertia system. Displacement (or acceleration) sensors are then required, corresponding to the number of degrees of freedom to extract eigenmode.

2.3 Identification and compensation of phase lag

In the last section, the basic formulation of mode-decoupled cutting force monitoring is presented. For high-precision and wideband cutting force monitoring, the phase shift between the signals, I_a^{ref}, θ_m, and x_t needs to be identified and compensated. Simultaneously, the accurate identification of modal parameters is also required. Figure 4 shows a schematic block diagram of the cutting force monitoring system with phase lag compensation. In the figure, two types of phase lag elements are considered. First, the bandwidth of the current control loop (5000 rad/s) was taken into account, and it was modeled as $H(s)(=\omega_{\text{cc}}/(s+\omega_{\text{cc}}))$. Second, the dead times in the control system were considered. Specifically, $e^{-T_a s}$ denoted the dead time of the servo driver, and the summation of delay in numerical differential and transmission of the encoder signal was modeled as $e^{-T_b s}$. Considering that $\hat{x}_m^{\text{res}}$ and $\hat{x}_t^{\text{res}}$ were delayed signals against I_a^{cmd}, the phase lag was compensated by delaying I_a^{cmd} so that the total amount of dead time became equal. Finally, a cutting force observer was constituted in each mode based on the compensated signals.

The measured and identified frequency response function (FRF) is shown in Fig. 5, and the identified parameters are listed in Table 1. Bandwidth of the current control loop (ω_{cc}) and dead time of servo driver (T_a) were determined from catalog value from manufactures. Dead time at encoder side (T_b) was experimentally determined so as to follow phase characteristics. Mechanical parameters were identified by applying differential iteration method [18], which was a sort of least square method in frequency domain. Non-linear terms of measured FRF were linearized by performing Taylor expansion around initial value. Modal parameters were iteratively calculated, while ω_{cc}, T_a, and

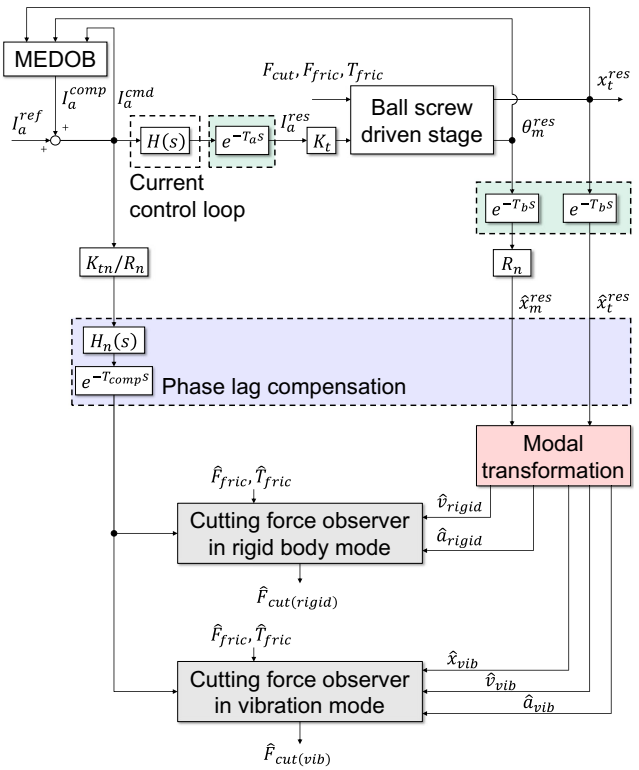

Fig. 4 Schematic block diagram of the cutting force estimation system in modal space with phase lag compensation

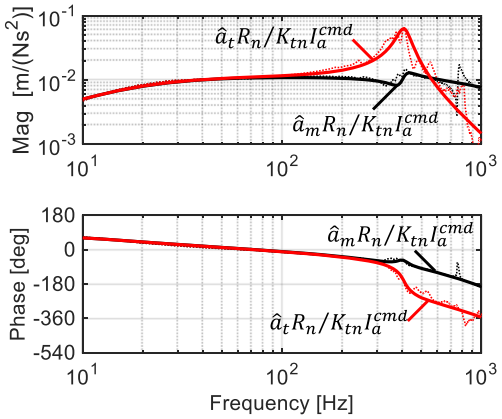

Fig. 5 Frequency response functions between motor thrust force and accelerations, $\hat{a}_m R_n / K_{tn} I_a^{\mathrm{cmd}}$, and $\hat{a}_t R_n / K_{tn} I_a^{\mathrm{cmd}}$ (*solid line*: model, *dashed line*: experimental)

T_b were excluded for iterative calculation. These parameters were used for the following simulation and experimental verifications.

3 Theoretical evaluation of monitoring performance

The estimated cutting forces were constituted from four forces (i.e., motor thrust, inertia, damping, and restoring forces). Assuming no modeling error, high precision and wideband cutting force monitoring was feasible, whichever estimating equations were applied. On the other hand, the proportion of the four forces used in estimating the cutting force varies responding to frequency, and it was different depending on the type of estimating equations. Thus, the estimation accuracy of the cutting force was influenced by the most dominant force. In this chapter, the proportion of each force was evaluated by a time domain simulation. In the simulation, a sinusoidal load force was applied as a command value. The FRF between the load force and each of the remaining forces was investigated by continuously varying the frequency of the applied force. The monitoring system was constructed based on Fig. 4. Note that, for the sake of simplification, the dead time elements, friction force, friction torque, and resolution of encoders were not considered. In order to attenuate higher frequency noise, a 4th order low pass filter (LPF) was implemented in the cutting force observer. The cutoff frequency of the LPF was set to 1000 Hz.

Table 1 Parameters for simulation and experiments

Total inertia of motor, coupling, and ball screw J_r [kg·m^2]	5.18×10^{-5}
Total movable mass M_t [kg]	6.55
Inertia ratio α [−]	0.080
Viscous coefficient of translational element C_t [N·s/m]	8.21×10^{2}
Damping coefficient of the mechanism C_k [N·s/m]	1.76×10^{3}
Viscous coefficient of rotational element D_r [N·m·s/rad]	6.50×10^{-3}
Total rigidity of feed screw system K_r [N/μm]	40.5
Dead time T_a, T_b [ms]	0.2, 0.2
Dead time for phase lag compensation T_{comp} [ms]	0.4

Figure 6 shows the gain characteristics between the applied load force and each of the remaining forces. In rigid body mode, the motor thrust force, $K_t I_a^{\mathrm{cmd}}/R$, consisted mostly of the estimated cutting force in lower frequencies. In higher frequencies, the contribution by the inertia force, $M_{\mathrm{rigid}}\hat{a}_{\mathrm{rigid}}$, increased, and therefore an accurate identification of inertia and the measurement of acceleration became important. The friction force and torque mostly consist of DC and low frequency components, and the motor thrust force (i.e., the current signal) is strongly affected by friction. Therefore, the motor thrust force component in the rigid body mode was subjected to friction as well as the conventional sensorless estimation technique using current signal. In the vibration mode, the proportion of motor thrust force, $\alpha K_t I_a^{\mathrm{cmd}}/R$, was lower because of the low inertia ratio (α: 0.080). Thus, the variation of the motor thrust force caused by friction affected less the estimation accuracy. On the other hand, the restoring force, $\alpha K_{\mathrm{vib}}\hat{x}_{\mathrm{vib}}$, was proportionally high in a wide frequency range. Accurate identification of stiffness was important in the vibration mode. When the frequency components close to the resonance frequency were monitored, the damping force, $\alpha C_{\mathrm{vib}}\hat{v}_{\mathrm{vib}}$, was non-negligible in the vibration mode.

4 Friction characteristics

To estimate the cutting force using Eqs. (5) and (6), the friction torque, T_{fric}, and friction force, F_{fric}, must be accurately identified and eliminated. As mentioned in the last chapter, the proportion of motor thrust force, $K_{tn} I_a^{\mathrm{ref}}/R_n$, became larger in lower frequencies in the rigid body mode. When the stage was moved at constant feed rate without additional load, such as the cutting force, the motor thrust force was assumed equal to

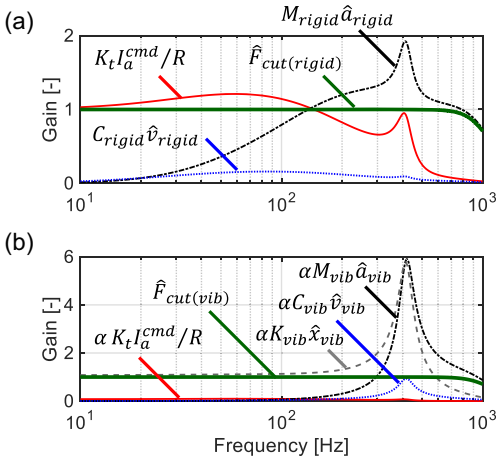

Fig. 6 Gain characteristics of each force **a** in rigid body mode and **b** in vibration mode

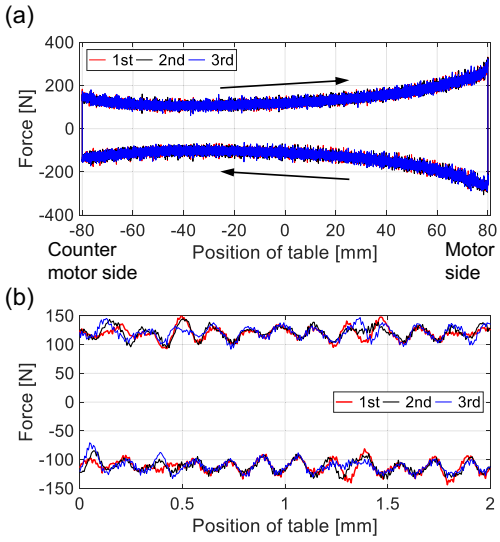

Fig. 7 Position-dependent and repeatable characteristics of friction force/torque at 20 mm/s **a** overall view and **b** expanded view

the summation of the friction force and friction torque, as could be noted from Eq. (5). Here, inertia and viscous terms were ignored. Figure 7 shows the friction characteristics identified by using the motor thrust force reference through the three experiments. The summation of the friction terms varied depending on the table position and fluctuated periodically at the same phase in each motion. The position-dependent fluctuation had high repeatability. The effect of the position-dependent friction on the cutting force estimation could be reduced by making use of the repeatability.

The frequency analysis results of the frictions were divided by feed rate in order to analyze the periodical fluctuation in

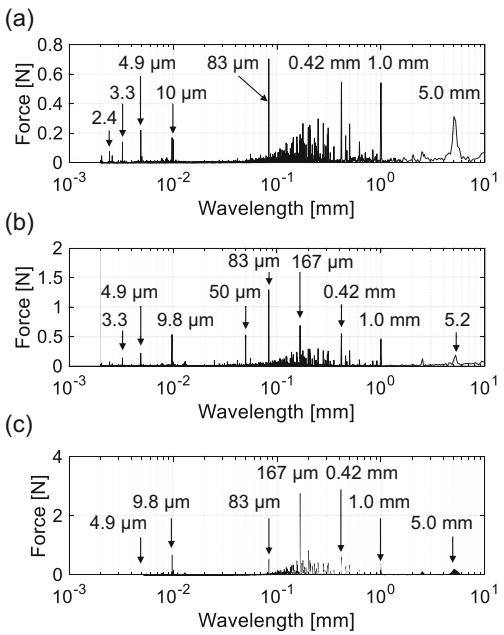

Fig. 8 Friction characteristics in wavelength domain at **a** 1 mm/s, **b** 5 mm/s, and **c** 20 mm/s

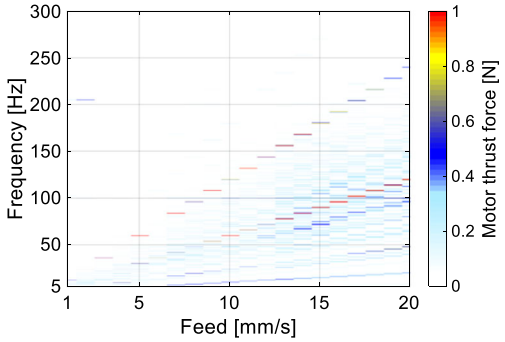

Fig. 9 Frequency analysis results of the motor thrust force at different feed rates

wavelength domain, and the results are presented in Fig. 8. Although the dominant components were different, multiple fluctuation components with the same wavelength were observed at different feed rates. The wavelength of the fluctuations ranged from the micrometer to millimeter regions. Disturbances in the mechanical system and in the control system including the servo motor could induce these fluctuations [11]. When the frequency of the fluctuation came close to that of the cutting force, the estimated cutting force might be distorted because of thrust force fluctuation. As shown in Fig. 9, the dominant frequencies in each feed rate linearly increased and were likely to approach the frequency of the cutting force. At the same time, the intensity of the spectrum was high with a higher feed rate. These results suggested that the feed rate could influence the estimation accuracy of the cutting force in the rigid body mode as well as the position-dependent fluctuations. In this study, however, the influence of the feed rate was not discussed.

On the other hand, as suggested by the simulation results in the vibration mode, the relative motion between rotation and translation had a larger influence on the estimation

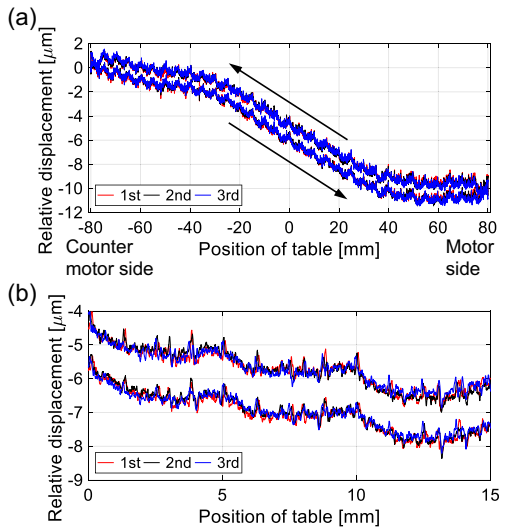

Fig. 10 Position-dependent and repeatable characteristics of relative displacement between motor angle and table response at 20 mm/s **a** overall view and **b** expanded view

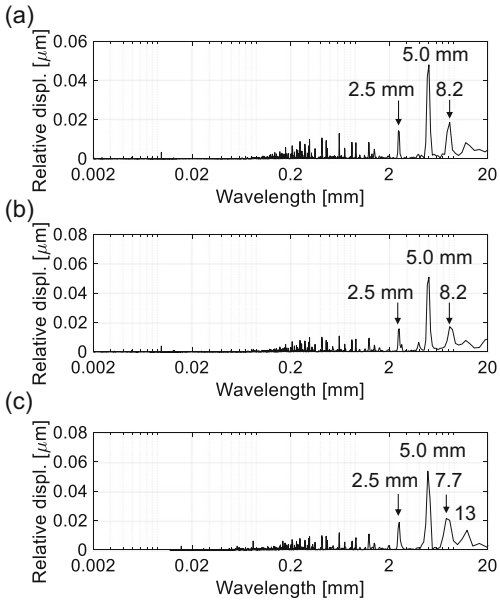

Fig. 11 Characteristics of relative displacement between motor angle and table response in wavelength domain at **a** 1 mm/s, **b** 5 mm/s, and **c** 20 mm/s

performance of the cutting force than the motor thrust force. Thus, the position-dependent characteristics of the friction terms were reflected in the relative displacement rather than in the motor thrust force. As shown in Fig. 10, the relative displacement has both position dependency and high repeatability, as in the case of the motor thrust force. On the other hand, the dominant wavelength of the relative displacement differed from that of the motor thrust force. The dominant fluctuation was in the millimeter region, as presented in Fig. 11, which suggested that lower frequency fluctuations were induced in the vibration mode. The fluctuation with a period of 5 mm presented the highest amplitude, which corresponded to the lead length of the screw.

Table 2 Experimental conditions

Spindle speed [min^{-1}]	1000, 4000, 10,000
Axial depth of cut [mm]	0.3
Radial depth of cut [mm]	6.0, 1.5
Type of immersion	Full immersion, quarter immersion down milling
Feed per tooth [μm/tooth]	30
Cutting tool	Square end mill
Tool diameter [mm]	ϕ 6.0
Number of flutes	2
Workpiece material	Al alloy (A5052)
Sampling frequency [kHz]	10
Cutoff frequency of LPF [Hz]	500
Type of LPF	Butterworse (4th order)
Cutoff frequency of MEDOB [Hz]	160

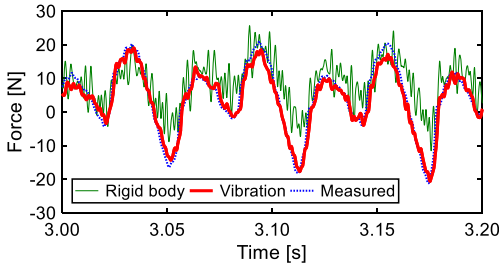

Fig. 12 Estimated cutting forces in feed direction (spindle speed 1000 min^{-1}, radial depth 6 mm)

Based on the position-dependent and repeatable characteristics, friction terms in each modal space were determined by idling (air cutting) tests in this study. Idling tests were performed three times before the cutting test in each cutting condition. In order to exploit position dependency, the position trajectory, and velocity in the idling test need to correspond as much as possible with those in the cutting tests. Stage weight including workpiece is also influencing factor on friction characteristics as well as stage position. In addition, mass variation of the workpiece can lead to estimation error of the cutting force especially in high frequencies, because frequency response of the feed drive is subjected to influence of the mass variation. On the other hand, the experimental setup is desktop size, and available mass is limited because of the table size. Therefore, discussion about stage weight is not included in experimental verification.

5 Experimental verification

5.1 Experimental conditions

For evaluating the monitoring performance of the mode-decoupled method, end milling tests were carried out using

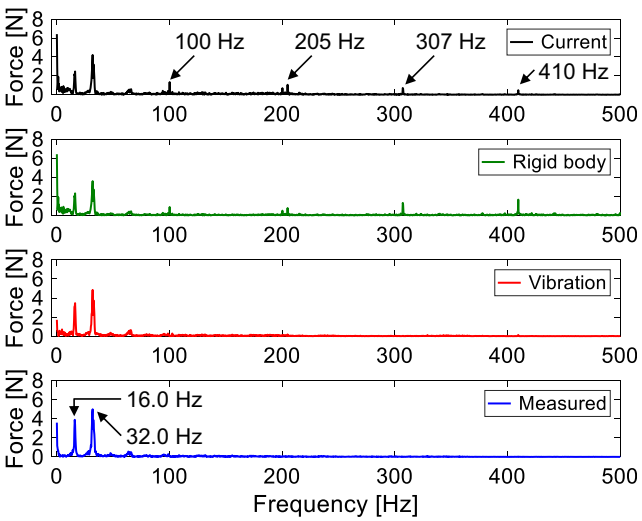

Fig. 13 Frequency analysis result of estimated cutting forces in feed direction (spindle speed 1000 min^{-1}, radial depth 6 mm)

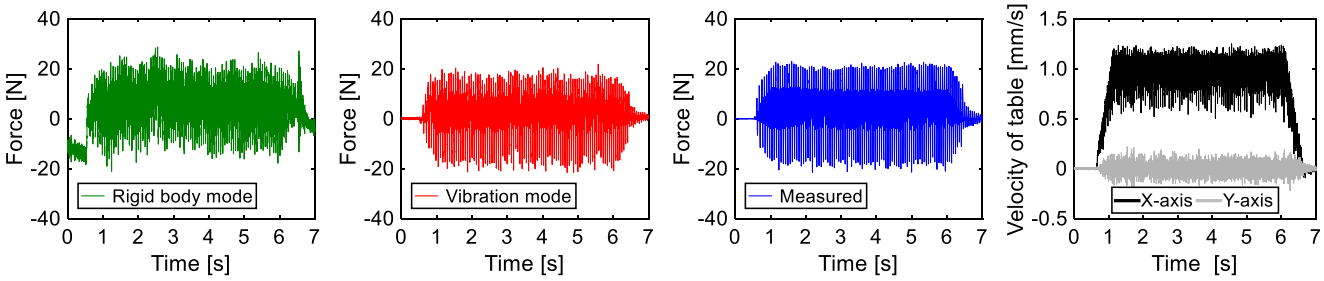

Fig. 14 Overall view of estimated cutting forces in feed direction and velocity response of table (spindle speed 1000 min^{-1}, radial depth 6 mm)

the prototype ball-screw-driven machine tool shown in Fig. 1. The cutting force monitoring system was installed in the control system of the *X*-axis ball-screw-driven stage. Table 2 summarizes the experimental conditions. In the end milling tests, the workpiece was machined at a constant feed rate and depth of cut. At first, the X-stage was moved, and the cutting force component in X-direction was monitored in order to evaluate the estimation performance in feed direction. Secondly, the *Y*-stage was moved, while the cutting force component in *X*-axis direction was monitored for evaluating the performance in cross-feed direction. As for load condition, we selected small axial depth of cut condition for the cutting force to become less than kinetic friction. This is because we aimed to show that smaller cutting force generated with a small depth of cut was observable. For fair comparison, both the estimated cutting force and the force measured by the dynamometer were filtered.

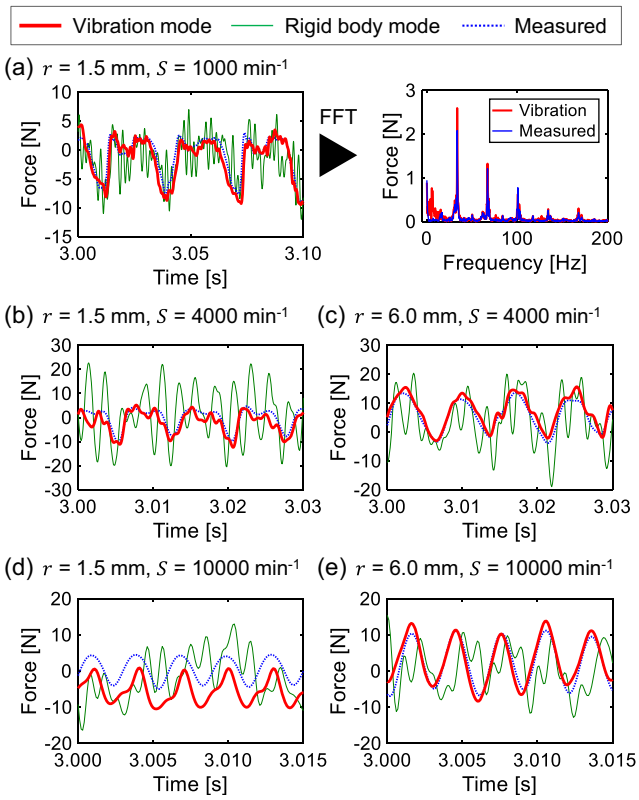

Fig. 15 Comparison of estimated cutting forces in feed direction with respect to radial depth and spindle speed. **a** $r = 1.5$ mm, $S = 1000$ min^{-1}. **b** $r = 1.5$ mm, $S = 4000$ min^{-1}. **c** $r = 6.0$ mm, $S = 1000$ min^{-1}. **d** $r = 1.5$ mm, $S = 10{,}000$ min^{-1}. **e** $r = 6.0$ mm, $S = 10{,}000$ min^{-1}

5.2 Experimental results and discussion

Figure 12 shows the experimental result at full immersion milling and 1000 min^{-1} spindle speed. Both of the estimated values could follow temporal variations during cutting. In the rigid body mode, however, the waveform was noisy, while the cutting force could be accurately estimated in the vibration mode. This is because high-frequency components, irrelevant to the cutting force, were included in the current reference (i.e., the motor thrust force reference). As shown in Fig. 13, four additional frequency components were included in both motor thrust force and estimated value in the rigid body mode: 100, 205, 307, and 410 Hz. Because the feed rate was 1 mm/s in this cutting condition, these frequency components corresponded to 10.0, 4.88, 3.28, and 2.44 fluctuations in the wavelength domain, respectively. These fluctuations were observed during the idling motion as presented in Fig. 8a. Because the signal period of the rotary encoder was 512 count/rev (i.e., 9.77 μm wavelength), these fluctuations were supposed to result from the angular measurement. On the other hand, longer-wavelength components, such as the per-83-μm variation (i.e., 12 Hz) were not observed in the rigid body mode. Similarly, longer-wavelength components were not induced in the vibration mode, while they were included in the relative displacement as shown in Fig. 11. The presented friction force/torque compensation method was particularly effective for eliminating longer-wavelength (i.e., low frequency) components, but was not necessarily valid for eliminating

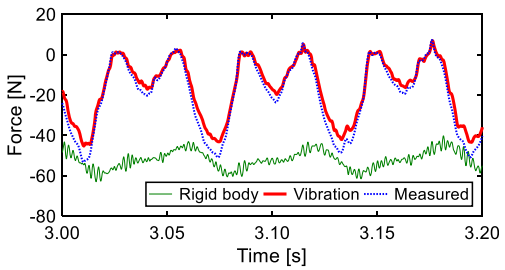

Fig. 16 Estimated cutting forces in cross-feed direction (spindle speed 1000 min^{-1}, radial depth 6 mm)

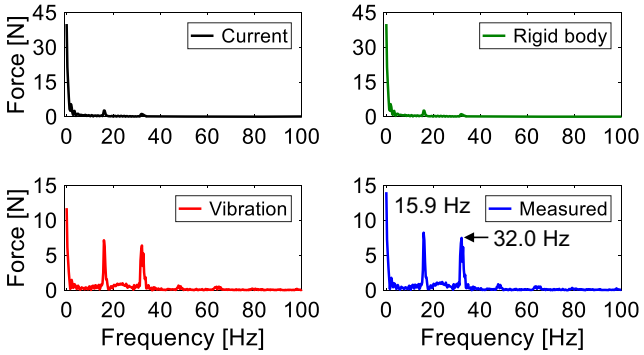

Fig. 17 Frequency analysis result of estimated cutting forces in cross-feed direction (spindle speed 1000 min^{-1}, radial depth 6 mm)

shorter-wavelength (i.e., high frequency) components. The fluctuation with shorter wavelengths needs to be eliminated by a suitable signal processing. When high repeatability existed, the cutting force components in the feed direction could be accurately estimated all the time, as shown in Fig. 14.

The monitoring performance of the cutting force was evaluated at different immersion and spindle speeds, and the results are presented in Fig. 15. As in the case of full immersion milling with 1000 min^{-1} spindle speed, higher frequency noises were included in the estimated value in the rigid body mode owing to angular measurement. Because the cutting process was more intermittent at quarter immersion milling (i.e., r = 1.5 mm), there were higher harmonics in the fast Fourier transform (FFT) result of the cutting forces, as shown in Fig. 15a. By estimating the cutting force components in the vibration mode, wideband cutting force monitoring including higher harmonics was possible. In the vibration mode, therefore, the cutting force could be accurately monitored, including that in the air-cutting region. The temporal variation of the cutting force could be accurately captured in the vibration mode at higher spindle speeds, as shown in Fig. 15b–e. In this regard, the estimation error in DC might happen because of the compensation error of friction terms, as shown in Fig. 15d.

In the next step, the monitoring performance of the cross-feed direction component of the cutting force was evaluated. The results in time domain and in frequency domain are presented in Figs. 16 and 17, respectively. In the rigid body mode, the DC component of the estimated value was far from that of the measured cutting force. The difference of the DC component was induced after the beginning of the cutting, as shown in Fig. 18. In addition, a temporal variation of the cutting force caused by tooth-pass was not reflected in the estimated value. On the other hand, by estimating the cutting force component in vibration mode, the cross-feed force components could be accurately estimated, as well as the feed force components.

The large estimation error in rigid body mode was attributed to the response of the motor thrust force. Because there was high repeatability and position dependency under constant feed motion, the motor thrust forces in cutting and in idling were partially overlapping, as shown in Fig. 19a. In this case, a motor thrust force of around 120 N was supplied in order to keep feed motion without stopping. Thus, the kinetic friction force of the X-stage was assumed to reach approximately 120 N. Figure 19b shows the cross-feed component of the motor thrust force, which was massed around −50 N during cutting and was smaller than the static friction force of the X-stage. Therefore, the presented motor thrust force corresponded to the static friction force of the X-stage. In this case, not the kinematic friction but the summation of the static friction and cutting forces approximately balanced the motor thrust force. However, the static friction force could not be acquired by the presented idling test as shown in Fig. 19b. Thus, it is difficult to estimate the cross-feed component of the cutting force in rigid body mode. When the cross-feed component of the cutting force is larger than the static friction force, it is possible to estimate the cutting force through frequency analysis of the motor thrust force [14]. However, the measured cutting force in cross-feed direction was less than the static friction force. In the rigid body mode, therefore, high precision cutting force monitoring in cross-feed direction was difficult.

Figure 20 shows the position response in cross-feed direction from the rotary and linear encoders. The waveform of the angle response in Fig. 20a was similar to that of the motor thrust force during cutting as shown in Fig. 19b. While the variation of the motor angle was comparatively small, a large position variation was observed at the table near the cutting point. In addition, the waveform of the table response was similar to the cutting force shown in Fig. 16, which indicates that the table response

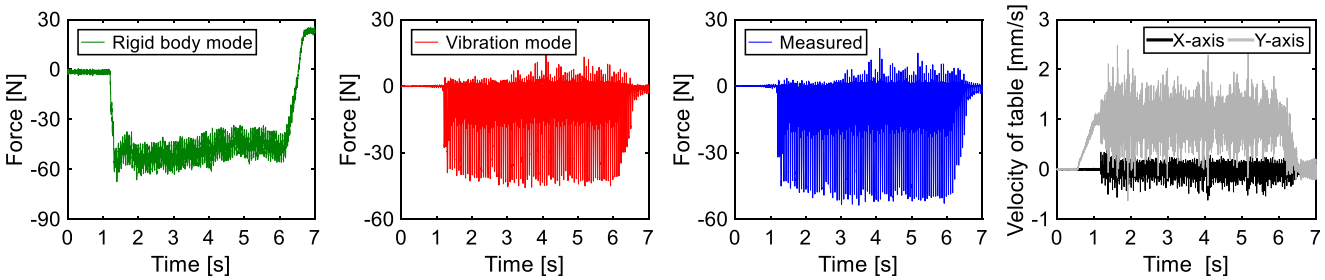

Fig. 18 Overall view of estimated cutting forces in cross-feed direction (X-axis) and velocity response of table (spindle speed 1000 min^{-1}, radial depth 6 mm)

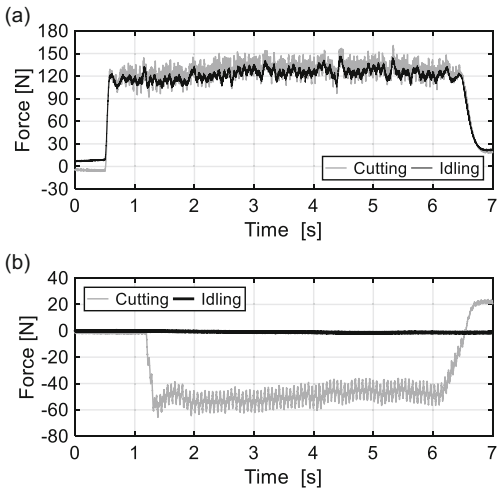

Fig. 19 Comparison of motor thrust force **a** in feed direction (1 mm/s) and **b** in cross-feed direction (stopped axis)

captured the dynamic variation of the cutting force. The DC component of the cutting force could not be extracted by only using the table response. By combining table and angle responses, an accurate cutting force monitoring, including the DC component, was accomplished in the vibration mode, even if the cutting force was less than the static friction force.

Figure 21 shows the estimation results of the cross-feed components with respect to radial depth of cut and spindle speeds. As in the case of feed force component, the dynamic variation of the cutting force could be accurately estimated in vibration mode. As mentioned before, the motor thrust force and the relative displacement fluctuated periodically, depending on the rotation/position when the feed motion was applied to the stage. However, the periodical fluctuation did not influence the estimation performance in cross-feed direction, because the stage was commanded to fix. Cutting force monitoring in vibration mode can offer higher estimation accuracy in cross-feed direction than in feed direction. When monitoring only cross-feed components of the cutting force, it was not necessary to perform idling tests before the cutting test, which we experimentally confirmed.

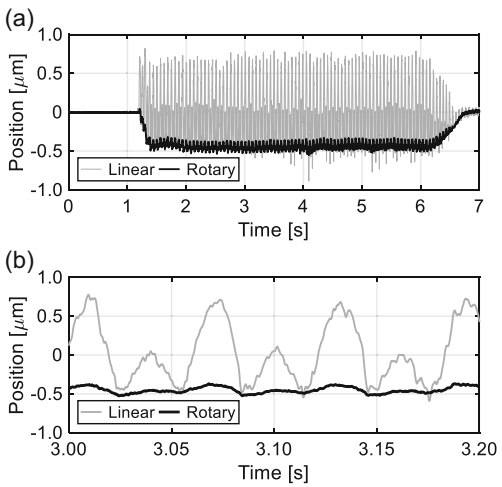

Fig. 20 Position response in cross-feed direction during cutting test at 1000 min^{-1} and 6.0 mm radial depth **a** overall view **b** expanded view

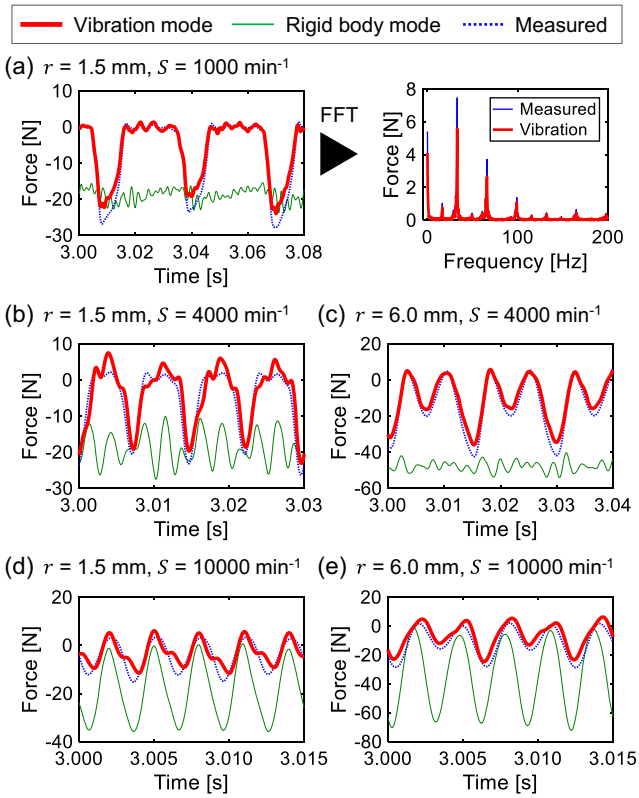

Fig. 21 Comparison of estimated cutting forces in feed direction with respect to radial depth and spindle speed. **a** $r = 1.5$ mm, $S = 1000$ min^{-1}. **b** $r = 1.5$ mm, $S = 4000$ min^{-1}. **c** $r = 6.0$ mm, $S = 4000$ min^{-1}. **d** $r = 1.5$ mm, $S = 10{,}000$ min^{-1}. **e** $r = 6.0$ mm, $S = 10{,}000$ min^{-1}

6 Conclusion

This study proposed a sensorless process monitoring technique by independently estimating the cutting force components in the rigid body and vibration mode coordinate systems, based on multi-encoder signals. The validity of the proposed cutting force monitoring technique was experimentally evaluated by end milling tests. The following conclusions can be drawn from the study:

1. The two mutually orthogonal modes were introduced from a dual-inertia model of the ball-screw-driven stage. In this method, the cutting force was estimated by using three pieces of servo information: motor current reference, motor angle, and displacement of the stage.
2. In the rigid body mode, the cutting force components were estimated by extracting the static rigid body motion, which was theoretically equivalent to cutting force monitoring applying the multi-encoder based disturbance observer. In the vibration mode, the cutting force was

estimated by using the relative displacement, velocity, and acceleration between the motor and the table.

3. Experimental results indicated that both estimation methods could extract temporal variation of the cutting force components in feed direction. In the rigid body mode, however, higher frequency variations irrelevant to the cutting force were included because of the periodical variation of the motor thrust force. In the vibration mode, an accurate and wideband estimation as sensorless approach was possible, including higher harmonics induced by intermittent cutting.
4. Cross-feed components of the cutting force less than the maximum static friction force were successfully estimated in the vibration mode. The relative motion-based estimation in the vibration modal space was more effective for monitoring cross-feed components than the motor thrust force-based estimation.

The proposed method is applicable to the *Y*-axis ball-screw-driven stage, which equips the spindle and the Z-stage. We experimentally confirmed that the cutting force components, both in feed and in cross-feed directions, were observable with low spindle speed. However, the estimation accuracy decreased with higher spindle speed, because the presented dual-inertia model did not consider the dynamics between the tool and the stage. The extension to a multi-inertia model, using additional displacement/acceleration sensors, is one of the solutions. In addition, the damping property of the guideway might be an important factor, which affected the position and angular response, especially in cross-feed direction. These factors are noteworthy for further accurate cutting force monitoring. In future work, we plan to evaluate estimation accuracy under pocketing operation with reciprocal motions. In addition, we also plan to apply the mode-decoupled cutting force monitoring method to the monitoring of chatter.

Acknowledgements This work was supported by JSPS KAKENHI, Grant Number 15H03904, NSK Foundation for the Advancement of Mechatronics. The authors would like to express their deepest appreciation to Toshiba Machine Co. Ltd. for the technical support to this research.

Appendix

Modal displacement in the rigid body mode is introduced by referring to Eq. (3) as follows:

$$x_{\text{rigid}} = \frac{1}{\alpha+1}(x_m + \alpha x_t) \tag{7}$$

Modal mass and damping in the rigid body mode are denoted by using parameters of the dual-inertia model as follows:

$$\begin{aligned} M_{\text{rigid}} &= M_r + M_t = (1+\alpha)M_r \\ C_{\text{rigid}} &= \alpha_c M_{\text{rigid}} = \alpha_c(1+\alpha)M_r \end{aligned} \tag{8}$$

The equation for cutting force in the rigid body mode (Eq. (5)) is rearranged by using Eqs. (7) and (8) as follows:

$$\begin{aligned} F_{\text{cut(rigid)}} &= \frac{K_t I_a^{\text{ref}}}{R} - (1+\alpha)M_r \cdot \frac{a_m + \alpha a_t}{\alpha+1} - \alpha_c(1+\alpha)M_r \cdot \frac{v_m + \alpha v_t}{\alpha+1} - \frac{T_{\text{fric}}}{R} - F_{\text{fric}} \\ &= \frac{K_t I_a^{\text{ref}}}{R} - M_r a_m - M_t a_t - \alpha_c M_r v_m - \alpha_c M_t v_t - \frac{T_{\text{fric}}}{R} - F_{\text{fric}} \\ &= \frac{K_t I_a^{\text{ref}}}{R} - M_r a_m - M_t a_t - C_r v_m - C_t v_t - \frac{T_{\text{fric}}}{R} - F_{\text{fric}} \end{aligned}$$

where

$C_r = \alpha_c M_r,$

$C_t = \alpha_c M_t$

The parameters for rotational elements written as translational terms (i.e., M_r, C_r, a_m, v_m) were rearranged to rotational terms (i.e., $J_r, D_r, \alpha_m, \omega_m$), and the estimating equation was as follows:

$$\begin{aligned} F_{\text{cut(rigid)}} &= \frac{K_t I_a^{\text{ref}}}{R} - \frac{J_r}{R^2} R\alpha_m - M_t a_t - \frac{D_r}{R^2} R\omega_m - C_t v_t - \frac{T_{\text{fric}}}{R} - F_{\text{fric}} \\ &= \frac{1}{R}\left(K_t I_a^{\text{ref}} - J_r\alpha_m - D_r\omega_m - T_{\text{fric}}\right) - M_t a_t - C_t v_t - F_{\text{fric}} \end{aligned}$$

The estimating equation in the rigid body mode is the same as that applying MEDOB, Eq. (6) in [15].

References

1. Teti R, Jemielniak K, O'Donnell G, Dornfeld D (2010) Advanced monitoring of machining operations. CIRP Ann - Manuf Technol 59:717–739. doi:10.1016/j.cirp.2010.05.010
2. Tlusty J, Andrews GC (1983) A critical review of sensors for unmanned machining. CIRP Ann - Manuf Technol 32:563–572. doi:10.1016/S0007-8506(07)60184-X
3. Albrecht A, Park SS, Altintas Y, Pritschow G (2005) High frequency bandwidth cutting force measurement in milling using capacitance displacement sensors. Int J Mach Tools Manuf 45:993–1008. doi:10.1016/j.ijmachtools.2004.11.028

4. Sarhan AAD, Matsubara A, Sugihara M et al (2006) Monitoring method of cutting force by using additional spindle sensors. JSME Int J Ser C 49:307–315. doi:10.1299/jsmec.49.307
5. Albertelli P, Goletti M, Torta M et al (2016) Model-based broadband estimation of cutting forces and tool vibration in milling through in-process indirect multiple-sensors measurements. Int J Adv Manuf Technol 82:779–796. doi:10.1007/s00170-015-7402-x
6. Altintas Y (1992) Prediction of cutting forces and tool breakage in milling from feed drive current measurements. J Eng Ind 114:386–392. doi:10.1115/1.2900688
7. Lee JM, Choi DK, Kim J, Chu CN (1995) Real-time tool breakage monitoring for NC milling process. CIRP Ann - Manuf Technol 44:59–62. doi:10.1016/S0007-8506(07)62275-6
8. Shinno H, Hashizume H, Yoshioka H (2003) Sensor-less monitoring of cutting force during ultraprecision machining. CIRP Ann - Manuf Technol 52:303–306. doi:10.1016/S0007-8506(07)60589-7
9. Takei M, Kurihara D, Katsura S, Kakinuma Y (2011) Hybrid control for machine tool table applying sensorless cutting force monitoring. Int J Autom Technol 5:587–593. doi:10.20965/ijat.2011.p0587
10. Kim GD, Chu CN (1999) Indirect cutting force measurement considering frictional behaviour in a machining centre using feed motor current. Int J Adv Manuf Technol 15:478–484. doi:10.1007/s001700050092
11. Kono D, Matsubara A, Shirai T et al (2016) Analysis of positional deviation caused by position-dependent disturbances in ball screw drive. J Japan Soc Precis Eng 82:589–594. doi:10.2493/jjspe.82.589
12. Jeong Y-H, Cho D-W (2002) Estimating cutting force from rotating and stationary feed motor currents on a milling machine. Int J Mach Tools Manuf 42:1559–1566. doi:10.1016/S0890-6955(02)00082-2
13. Ibaraki S, Sakahira M, Saraie H et al (2004) On the monitoring of cutting forces in end milling processes: an estimation method by geometrically combining force vectors of servo motors and a spindle motor. J Japan Soc Precis Eng 70:1091–1095. doi:10.2493/jspe.70.1091 (in Japanese)
14. Sato R, Hasegawa M, Keiichi S (2013) Cutting force monitoring based on the frequency analysis of feed motor torques. J SME Japan 2:7–12
15. Yamada Y, Kakinuma Y (2016) Sensorless cutting force estimation for full-closed controlled ball-screw-driven stage. Int J Adv Manuf Technol 87:3337–3348. doi:10.1007/s00170-016-8710-5
16. Mitsantisuk C, Nandayapa M, Ohishi K, Katsura S (2013) Design for sensorless force control of flexible robot by using resonance ratio control based on coefficient diagram method. Autom – J Control Meas Electron Comput Commun 54:62–73. doi:10.7305/automatika.54-1.311
17. Matsubara A, Lee K, Ibaraki S et al (2004) Enhancement of feed drive dynamics of NC machine tools by actively controlled sliding guideway. JSME Int J Ser C 47:150–159. doi:10.1299/jsmec.47.150
18. Van Loon P (1974) Modal parameters of mechanical structures. Ph.D dissertation, K.U. Leuven